Boundary-Layer Meteorol (2007) 122:31–41
DOI 10.1007/s10546-006-9092-2

ORIGINAL PAPER

Sea-breeze scaling from numerical model simulations, part II: Interaction between the sea breeze and slope flows

Aurore Porson · Douw G. Steyn · Guy Schayes

Received 29 September 2005 / Accepted 14 April 2006 /
Published online: 21 October 2006

Abstract Numerical model simulations of sea-breeze circulations in the presence of idealized topography are subjected to dimensional analysis in order to capture the dynamics of the sea-breeze circulation combined with an upslope-flow circulation. A secondary objective is to reconcile previous results based on observations. The analysis is based on a scaling analysis of sea-breeze speed, depth and volume flux. This study is motivated by the fact that the literature of sea breezes interacting with upslope flows is generally qualitative. Results show clear scaling regimes and strong interaction between the two thermally driven circulations. We distinguish three regimes, depending on slope length, slope angle, stability and surface heat flux. The first and third regimes obey the scaling laws of pure sea-breeze scaling. The second regime shows a significant decrease in the scaled volume flux relative to pure sea-breeze scaling. Dynamical relations in the second regime show a strong influence on the circulation of upslope stable air advection.

Keywords Numerical model · Scaling analysis · Sea breeze · Slope flow · Stability · Surface heat flux

1 Introduction

Existing studies of sea breezes combined with slope flows present two distinct, and seemingly, contradictory results. Mahrer and Pielke (1977), Estoque (1981), Estoque and Gross (1981) and Banta and Olivier (1993) showed that the presence of upslope flows results in sea breezes having greater inland penetration than pure sea breezes.

A. Porson (✉) · G. Schayes
Institut d'Astronomie et de Géophysique Georges Lemaître, Université Catholique de Louvain, Brussels, Belgium
e-mail: porson@astr.ucl.ac.be

D. G. Steyn
Department of Earth and Ocean Sciences, University of British Columbia, Vancouver, BC, Canada

Lu and Turco (1994) and Hadi et al. (2002), however, showed that the inland extent and speed of the combined circulation depends on the vertical potential temperature profile and, in the case of strong gradients, the combined circulation can be blocked by mountains.

We will attempt to link these two conflicting effects, mainly evident in the inland extent, to the dependence of the intensity of the combined circulation on the governing variables. In order to achieve our objectives, we will use non-linear numerical simulations with idealized topography and boundary conditions to simulate sea-breeze circulations in the presence of slope circulations. Our analysis will be an extension of that presented in Steyn (2003) and Porson et al. (2006), and will use the mesoscale model TVM as the primary research tool (Schayes et al. 1996, Thunis and Clappier 2000). We will use empirical scaling analysis of model output to capture the governing relations of sea breezes in the presence of simple topography. A sloping coastal plain of a given slope angle and slope length will be used, and slope length will initially be taken as 130 km (the influence of slope length is investigated in Section 4). Simulations will use different vertical stability (the initial potential temperature gradient γ varies from 1.65 to 6.15 K km^{-1}) and slope angles (from 0° to 2.3°). Behind the slope, the height of the surface is constant for two grid points (6 km) for the treatment of the boundaries with zero-gradient. We will also interpret our results in relation to the analytical study of Kuwagata and Kondo (1989).

Our specific objectives are:

- How can we incorporate the influence of topography in the scaling laws derived for a pure sea-breeze circulation?
- How is the interaction between sea breeze and slope flow reflected in the scaling laws?
- How do the results of this scaling analysis compare to previous results on sea breezes in the presence of topography, and how can they be extended to realistic cases?

2 Combined sea breezes and upslope flows

For insight into how model simulations capture the three types of circulation (sea breeze, slope flow and combined sea breeze and slope flow), Fig. 1 illustrates the horizontal wind component for the three types as a function of distance from the coastline at 1500 LST. Geostrophic wind is zero and the simulations are presented for the stability group γ_5. The sea-breeze circulation is seen to exist over a much shorter distance inland, and when there is no longer the sea-breeze circulation, the slope-flow circulation is identical to the combined circulation. The model results show that in the afternoon, the combined sea-breeze and slope-flow circulation has a maximum intensity near the coastline and a depth that increases progressively from the coastline. The maximum intensity is found where the depth of the combined breezes undergoes a marked increase. This behaviour is shown in Fig. 2 for two values of the initial stability ($\gamma_1 = 1.65$ K km^{-1} and $\gamma_{10} = 6.15$ K km^{-1}), zero geostrophic wind, at 1500 LST. The increase in flow depth from the coastline marks the inland intrusion of marine air, and is evident since this increase was not present in the simulations of pure upslope flows. Lu and Turco (1994) reported this effect in the form of lower coastal boundary-layer depths due to the progression of marine air by sea breezes.

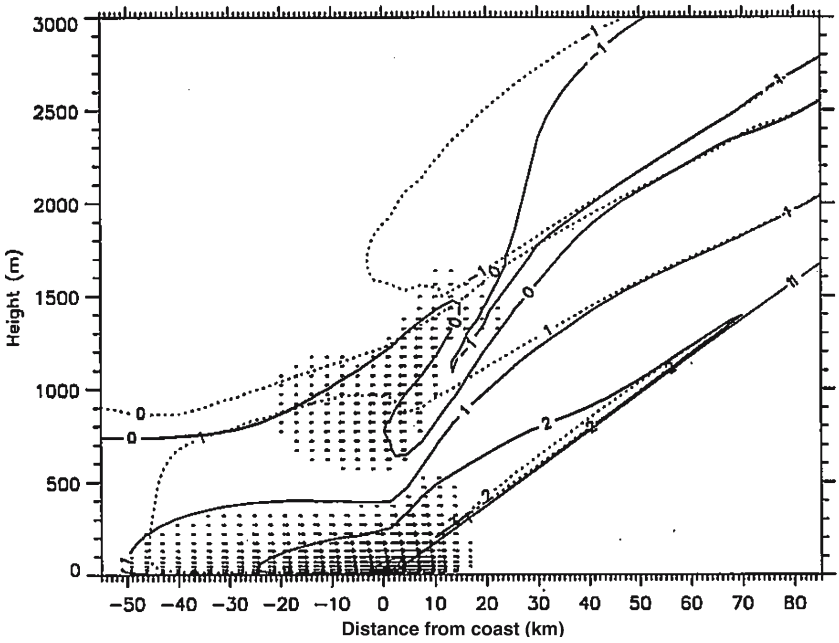

Fig. 1 Horizontal wind component of the three types of circulation: sea breeze (arrows), slope flow (solid line) and combined sea breeze and slope flow (dotted line) in a vertical plane along the west-east direction. This is done for the stability group γ_5 and a slope angle of 1.14° for the slope-flow and combined circulations

The strength of the combined breezes should then be measured where the flow depth undergoes the increase, and therefore the maximum intensity will be used here to represent the strength of the combined circulation; this variable is called U_{sbslope}. U_{sbslope} will then be the maximum along the slope of the vertically integrated speed of the combined circulation.

3 The influence of slope angle on sea-breeze and slope-flow scaling

3.1 Identification and characteristics of the three regimes

Following Porson et al. (2006) and introducing topography with a fixed slope length, the scaling is now based on five parameters (the buoyancy parameter g/T, the time-averaged integrated heat flux H, the Earth's diurnal rotational frequency ω, the Brunt–Väisälä frequency N and the slope angle α), incorporating three fundamental dimensional units (length, time and temperature). Within the framework of the Buckingham Pi theorem, this leads to two non-dimensional groups Π_4 (N/ω) and Π_5 (α). This approach will avoid any hidden correlation for the scaling analysis of the wind speed since the velocity scale and the two non-dimensional groups Π_4 and Π_5 are totally independent of each other. Concerning the analysis of the volume flux, the results will be compared to the analytical study of Kuwagata and Kondo (1989).

The TVM model is then run with different initial conditions capturing eight slope angles α_j, $j = 1,8$: $\alpha_1 = 0.076°$, $\alpha_2 = 0.23°$, $\alpha_3 = 0.38°$, $\alpha_4 = 0.77°$, $\alpha_5 = 1.14°$,

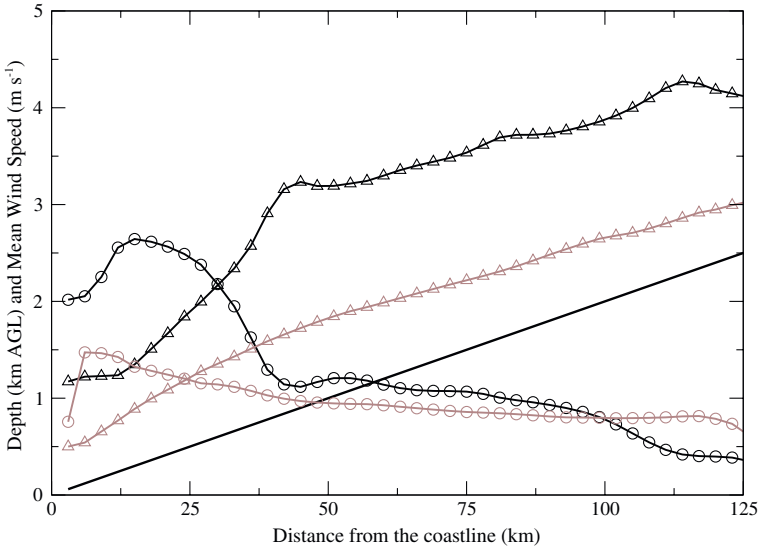

Fig. 2 Mean wind speed ($\mathrm{m\,s^{-1}}$) and depth as a function of distance from the coastline (km) at 1500 LST. Circulation depth is defined as the above-ground height at which the horizontal velocity component in the cross-shore direction first reaches zero. Mean speed is indicated with circles and the depth with triangles. This is done for two groups of stability γ_1 and γ_{10}, depicted respectively in black and grey. The topographic slope used here is represented by a thick black line

$\alpha_6 = 1.53°$, $\alpha_7 = 1.9°$, $\alpha_8 = 2.3°$ and 10 stability values : γ_i (in $\mathrm{K\,km^{-1}}$) $= 1.65 + 0.5i$ with $i = 0, 9$. The geostrophic wind is zero.

A multiple regression analysis on the scaled speed $U_{\mathrm{sbslope}}/u_{\mathrm{sscale}}$ and volume flux $VF_{\mathrm{sbslope}}/VF_{\mathrm{scale}}$ yields three distinct regimes with increasing slope angles and stability. We will call these Regimes I, II and III. The extreme regimes (Regimes I and III) have identical patterns of scaled speed and volume flux. The scaling that characterizes these two extreme regimes is similar to pure sea-breeze scaling from Porson et al. (2006). In these two regimes, the combined circulations achieve an equilibrium between the advection of stable air from the sea surface and the accumulated convergence of heat over land since sunrise at a fixed time in the afternoon. Regime III is, however, characterized by a lower balance of these two terms than in Regime I, as explained later. A first explanation is that as the slope or stability increase, the air in the upslope flow becomes progressively cooler relative to the air outside the flow, but remains warmer.

In Regime II, the scaled speed and volume flux decrease with increasing stability and slope angle or decreasing surface heat flux. The rate of decrease is close to that found in the analytical study of Kuwagata and Kondo (1989), who specify zero heat flux over all surfaces adjacent to the slope. In these conditions, the study of Kuwagata and Kondo (1989) can be used to understand the dynamics of sea breezes in combination with slope flows. They gave the speed in steady conditions U_{equi} as,

$$U_{\mathrm{equi}} \approx Q_{\mathrm{s}}^{1/2} \left(\frac{g}{T\gamma \sin(\alpha) C_M} \right)^{1/4}, \tag{1}$$

and the volume flux VF_{equi} as,

$$VF_{\text{equi}} = U_{\text{equi}}\, h_{\text{equi}} = \frac{Q_{\text{s}}}{\gamma \sin(\alpha)} \tag{2}$$

with h_{equi} the height at the equilibrium, Q_s the surface heat flux (kept constant during the day) and C_M the drag coefficient. Note that Eq. (1) results in a speed similar to that obtained by Schumann (1990) in a large-eddy simulation study.

According to Eq. (1), the scaled speed as a function of Π_4 and Π_5 should be:

$$\frac{U_{\text{sbslope}}}{u_{\text{sscale}}} \approx \Pi_4^{-1/2} \Pi_5^{-1/4} \tag{3}$$

with $u_{\text{sscale}} = (gH/T\omega)^{1/2}$, and according to Eq. (2) the scaled volume flux should be:

$$\frac{VF_{\text{sbslope}}}{VF_{\text{scale}}} \approx \Pi_4^{-1} \Pi_5^{-1} \tag{4}$$

with $VF_{\text{scale}} = gH/T\omega N$. Figures 3 and 4 show respectively the three regimes (Regimes I, II and III) for the scaled speed and volume flux from TVM as a function of Eqs. (3) and (4). In Regime II, the wind speed and volume flux follow the regressions in Eqs. (3) and (4). In Regime II, the scaled speed gives a multiplicative coefficient of 3.01 with a standard error of the estimate of 0.01 and the scaled volume flux gives a coefficient of 26.2 with a standard error of the estimate of 1.4. In the two extreme regimes (Regimes I and III), the scaled wind speed and volume flux are constant. The regression on sea-breeze and slope-flow speed scaling in Regime II can be further improved by focusing on the points centered in the area of decrease, but the significance of the regression might then be influenced by the reduced amount of model data. The scaled volume flux decreases in Regime II over a shorter range of slope angles than the scaled speed due to relatively constant depths at the boundary with Regime I. From Figs. 3 and 4, at the limit of very small slope angles, the combined sea-breeze and slope-flow circulation is found in Regime I and, therefore, does not obey the scaling laws of Kuwagata and Kondo. The reason is that the upslope-flow circulation has, by this time, yet to develop fully, as will be explained shortly. In Fig. 4, the scaled volume flux asymptotically follows the behaviour reported in Kuwugata and Kondo (1989).

These three scaling regimes also correspond to a particular behaviour of the inland position of the maximum updraft velocity (to a good approximation, this position identifies the location of the frontal zone of the combined circulation). Figure 5 shows how the inland position of the maximum updraft velocity is related to the separation between the three regimes. A strong intensification effect is detected in Regime I and a strong blocking effect in Regime II. These two competing effects have been mentioned previously, e.g. in Banta and Olivier (1993) and Lu and Turco (1994), and can now be understood in terms of the characteristics of Regimes I, II and III.

3.2 The nature of the equilibrium in Regime III

One possible mechanism that explains the decrease in volume flux detected in Regime II is related to the blocking/mechanical effect of the topography. This explanation derives from the slope-angle dependence detected in Regime II from Eqs. (3) and (4). Another possible mechanism for this decrease can be arrived at by viewing Regime II as a transition between Regimes I and III, both of which maintain an equilibrium

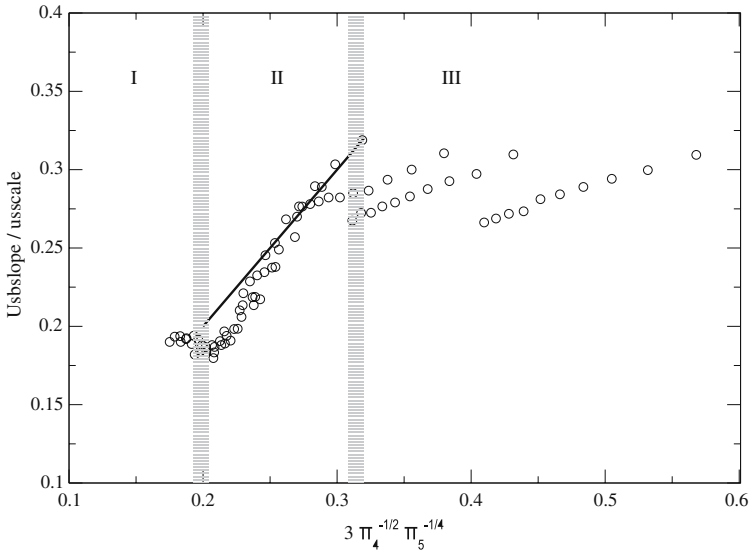

Fig. 3 TVM data for $[U_{\text{sbslope}}/u_{\text{sscale}}]$ as a function of the regression in Eq. (3). The 10 groups of stability, γ_1 to γ_{10} are illustrated for eight slope angles from α_1 to α_8. On the x-axis, the highest (smallest) slope angle values are found on the left (right). The black line indicates the one to one line derived from Kuwagata and Kondo (1989). Boundaries between the three regimes are illustrated by vertical lines

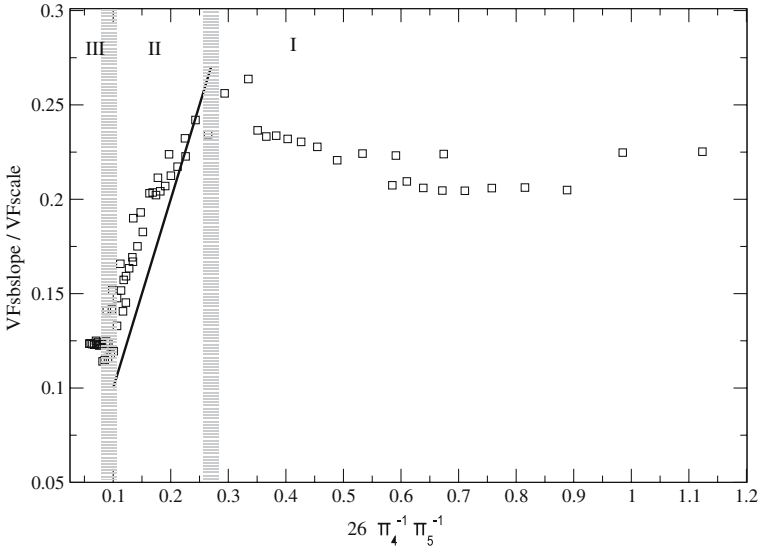

Fig. 4 TVM data for $[VF_{\text{sbslope}}/VF_{\text{scale}}]$ in Regimes II and III as a function of the regression Eq. (4). The 10 groups of stability, γ_1 to γ_{10} are illustrated for eight slope angles $\alpha_1 = 0.076°$, $\alpha_2 = 0.23°$, $\alpha_3 = 0.38°$, $\alpha_4 = 0.77°$, $\alpha_5 = 1.15°$, $\alpha_6 = 1.53°$, $\alpha_7 = 1.9°$, $\alpha_8 = 2.3°$. On the x-axis, the highest (smallest) slope angle values are found on the left (right). The black line indicates the one to one line derived from Kuwagata and Kondo (1989). Boundaries between the three regimes are illustrated by vertical lines

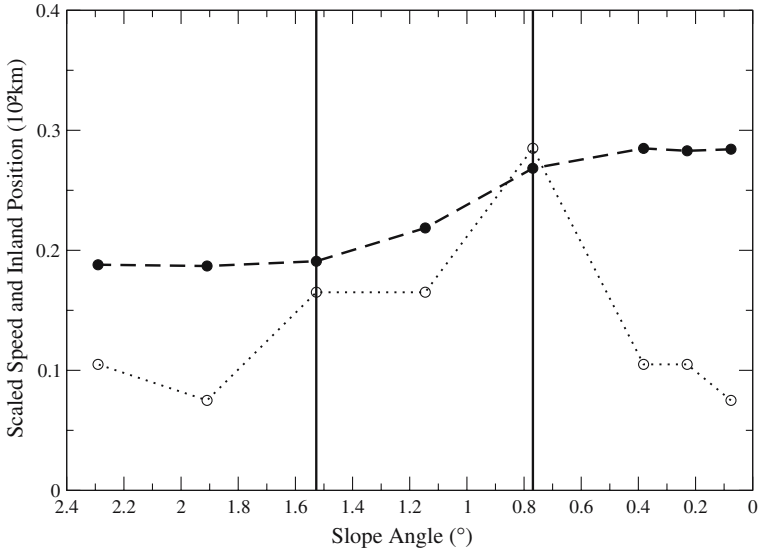

Fig. 5 TVM data for $[U_{\text{sbslope}}/u_{\text{sscale}}]$ (dashed line) and of the horizontal extent (dotted line) as a function of slope angle. This is done for the stability group γ_5

between stable air advection $VF_{\text{sbslope}} \times N$ and heat convergence $gH/T\omega$. Let us consider the intermediate stability value γ_5. Figure 6 shows the vertically averaged horizontal speed of the circulation along the slope for this case. The maximum speed is detected near the coastline and decreases strongly between slope angles α_4 and α_6 as captured by Eq. (3). Another feature evident in Fig. 6 is the growth of the circulation along the slope from α_3 to α_4, just before Regime II. This growth of the circulation along the slope disrupts the equilibrium in Regime I (by allowing larger advection of stable air) and forces the circulation to move to Regime II and then III where it again achieves an equilibrium between $VF_{\text{sbslope}} \times N$ and $gH/T\omega$ but with a lower coefficient.

The equilibrium in Regime III is related to the growth of the upslope-flow circulation. The lower coefficient in the Regime III equilibrium is supported by Darby et al. (2002) who found that upslope flows alone have lower speeds than upslope flows combined with sea breezes. The mechanism whereby growth of the upslope-flow circulation characterizes Regime II, and leads to a lower balance in Regime III, can be approached by considering the results of Chen et al. (1996), who discovered that the speed of upslope flows is larger at a given slope angle when ambient stability is stronger. According to this result, the growth of the upslope-flow circulation and its link to Regime II is then more significant at a given slope angle when ambient stability becomes stronger, which explains the dependence on stability detected in Regime II.

According to Eqs. (3) and (4), the equilibrium in Regime III is obtained at smaller slope angles when ambient stability becomes larger, which is similar to the result of Vergeiner and Dreiseitl (1987) and Vergeiner (1991) who, in a study of slope flows, pointed out the importance of convective motions (weaker when stability is larger) for driving slope flows away from equilibrium.

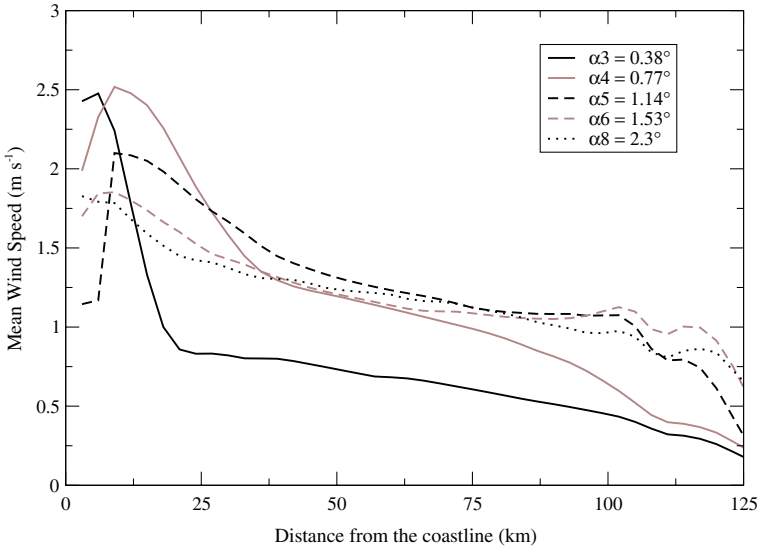

Fig. 6 Mean wind speed along the slope for different slope angles. This is done for the group γ_5

A similar sequence of regimes can be found in Haiden's (1990) work on slope flows. Haiden (1990) found that for slope angles larger than approximately 5.7° (on the order of 10%), the upslope flow speed is independent of stability and slope angle (as in Eq. (3)). This value of 5.7° is larger than the values of slope angle used here, but a similar value can be obtained when slope lengths become shorter, as in the following section.

The similarity between the present work and earlier studies of slope flows allows us to qualify Regime I as a regime dominated by the sea-breeze circulation, Regime III as a regime dominated by the upslope-flow circulation and Regime II as a regime of strong interaction between the two circulations.

4 The influence of slope length on sea-breeze/slope-flow scaling

In order to investigate these effects in more realistic cases, the three regimes and their characteristics are now investigated for shorter slope lengths than 130 km. TVM was run for eight slope angles α_j, for three groups of stability γ_1, γ_5 and γ_{10} and for a slope length range of [25, 45, 75, 100] km (the slope angle range was further extended for the smallest slope lengths).

The three regimes are still evident and appear in the same way as they do for longer slope lengths but are displaced to larger slope angles. This behaviour is illustrated in Fig. 7. When slope height at a given slope angle, or equivalently slope length, is reduced, the three regimes are found towards the left part of the regime diagram, thus for larger slope angles. For example, for a slope length of 25 km, Regime III occurs for a slope angle of 6.9° for the group γ_1, for a slope angle of 3.9° for the group γ_5 and for a slope angle of 2.7° for the group γ_{10}.

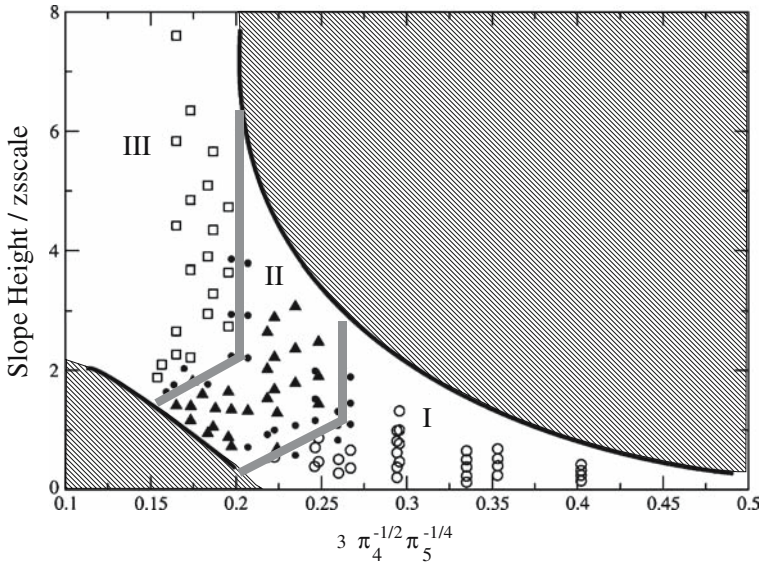

Fig. 7 Regime diagram in the space defined by scaled speed from Eq. (3) and [*Slope height*/z_{sscale}]. Thick grey lines, representing regime boundaries, were drawn to follow the small filled circles which denote model output at boundaries of two of the three regimes. Model outputs in Regime I are illustrated by large circles, in Regime II by filled triangles and in Regime III by squares

We are now in a position to examine more comprehensively agreement with results from the analytical study of Kuwagata and Kondo (1989) than was possible in Section 3. Kuwagata and Kondo also distinguished different zones (their term) or regimes (our term) that were depicted in a scaling diagram by plotting slope height/h_{equi} on the x-axis and $\sin(\alpha)$ on the y-axis. In their zones I (the quasi-equilibrium for which $u = U_{\text{equi}}$, a constant and $h = h_{\text{equi}}$, a constant) and II, momentum advection and shear stress balance respectively the horizontal pressure gradient and buoyancy flux. However, in zone I, both momentum advection and pressure gradient are zero, and the equilibrium is found between the advection of γ and surface heat flux (as in Eq. (2)). In zone III, for larger slope angles relative to zone I, the momentum advection becomes dominant and balances the pressure gradient and buoyancy. In zone IV, for smaller slope angles, shear stress is the only force retarding upslope flows, and balances the pressure gradient.

To compare the two studies further, Fig. 8 plots Regimes I, II and III on the zone diagram of Kuwagata and Kondo (1989). Regime I (filled circles) is mostly detected inside zones II and IV and Regimes II and III inside zone I. The shaded circles indicate model data located at the boundary between Regimes I and II. The present work therefore extends the study of Kuwagata and Kondo (1989) since:

– The flow dependence on slope length is explained here by the existence of three regimes. Indeed, for shorter slope lengths, Regimes II and III are obtained at larger slope angles resulting in a flow dependence on slope length for a given slope angle.
– The existence of these three regimes demonstrates why the dependence on slope length is more important for weaker stability cases than stronger stability cases. In weaker stability cases, the flow attains the equilibrium in Regime III at larger slope angles than in stronger stability cases.

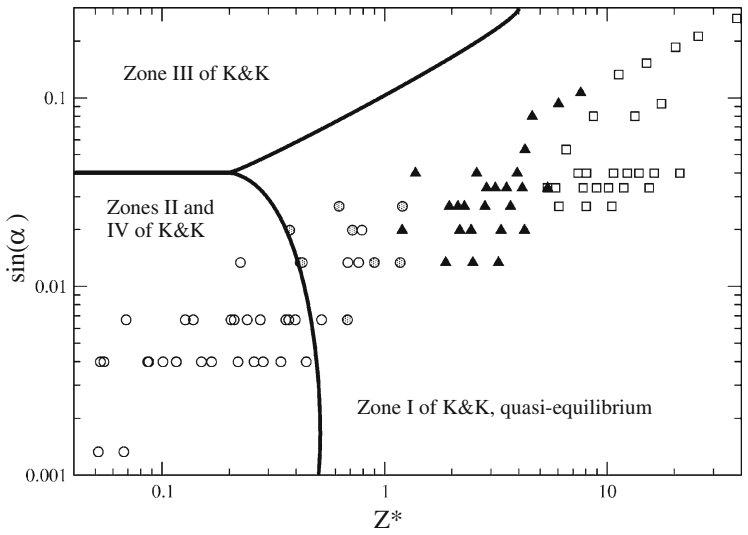

Fig. 8 Model data for Regimes I (circles), II (filled triangles) and III (squares) on the regime diagram of Kuwagata and Kondo. $Z^* =$ slope height/h_{equi}. Boundaries between the different zones of Kuwagata and Kondo's diagram are given as thick lines. The shaded circles represent model outputs at the boundary between Regimes I and II

– The quasi-equilibrium zone in Kuwagata and Kondo (1989) is here divided in two parts: a transition (Regime II) and an equilibrium (Regime III). In Regime II, similar speed and volume flux scalings are obtained in both studies.

5 Conclusions

The present study has extended the pure sea-breeze scaling to combined sea breezes and slope flows by using non-linear numerical model simulations in a coastal domain with idealized topography. Dependence on topography was investigated by varying slope angles and slope lengths of a simple slope in the coastal zone.

With varying slope angles, an analysis of the scaled speed and volume flux lead to the definition of three regimes, respectively Regimes I, II and III. These regimes are characterized by the different inland extent of maximum updraft velocity (frontal position), and are subject to different scaling laws. Regimes I and III obey the equilibrium scaling conditions identified for pure sea breeezes by Porson et al. (2006). Regime II is a transition regime in which the volume flux strongly decreases with governing variables. This effect is due to a strong growth in the upslope-flow circulation within the regime.

The similarity of the Regime I results to published work on sea breezes, and of the Regimes II and III results to published work for slope flows, allows us to characterize Regime I as capturing a combined circulation in which sea breezes dominate, and Regime III as the combined circulation in which slope flows dominate, with Regime II, the transition between these two states.

Varying slope lengths to obtain more realistic cases, the study compares closely to the analytical study of Kuwagata and Kondo (1989) with their quasi-equilibrium

zone resolved into two regimes. The dependence on slope length from Kuwagata and Kondo (1989) is further explained by the displacement of Regimes I, II and III at larger slope angles.

Acknowledgements This study was supported by Fonds pour la Formation à la Recherche dans l'Industrie et dans l'Agriculture, Belgium and the Natural Science and Engineering Research Council of Canada, the Belgian National Fund for Research and the French Community of Belgium. Special thanks are due to Alberto Martilli and Terry Clark for help with modelling questions.

References

Banta RM, Olivier LD (1993) Evolution of the monterey bay sea-breeze layer as observed by pulsed doppler lidar. J Atmos Sci 50:3959–3982

Darby LS, Banta RM, Pielke RA (2002) Comparisons between mesoscale model terrain sensitivity studies and doppler lidar measurement of the sea breeze at monterey bay. Mon Wea Rev 130:2813–2837

Chen RR, Berman NS, Boyer DL, Fernando HJS (1996) Physical model of diurnal heating in the vicinity of a two-dimensional ridge. J Atmos Sci 53:62–85

Estoque MA (1981) Further studies of a lake breeze part I. Mon Wea Rev 109:611–618

Estoque MA, Gross JM (1981) Further studies of a lake breeze part II. Mon Wea Rev 109:619–634

Hadi RW, Horinouchi T, Tsuda T, Hashiguchi H, Fukao S (2002) Sea-breeze circulation over Jakarta, Indonesia: a climatology based on boundary-layer radar observations. Mon Wea Rev 130:2153–2165

Haiden T (1990) Analytische Untersuchungen zur Konvektiven Grenzschicht im G ebirge. Ph.D Dissertation, Universitt Wien, Austria, 140 pp

Kuwagata T, Kondo J (1989) Observation and modeling of thermally induced upslope flow. Boundary-Layer Meteorol 49:265–293

Lu R, Turco RP (1994) Air pollutant transport in a coastal environment. part I: two-dimensional simulations of sea-breeze and mountain effects. J Atmos Sci 51:2285–2308

Mahrer Y, Pielke RA (1977) The effects of topography on sea and land breezes in a two-dimensional numerical model. Mon Wea Rev 105: 1151–1161

Porson A (2005) Sea breeze scaling in idealized conditions: the influence of topography and large-scale winds. Ph.D Dissertation, Université catholique de Louvain, Louvain-la-Neuve, Belgium, 259 pp

Porson A, Steyn DG, Schayes G (2006) Sea-breeze scaling from numerical model simulations, part I: Pure sea breezes. Boundary-Layer Meteorol in press.

Schayes G, Thunis P, Bornstein R (1996) Topographic vorticity-mode mesoscale-beta (TVM) model. Part I : formulation. J Appl Meteorol 35:1818–1823

Schumann U (1990) Large-eddy simulation of the upslope boundary-layer. Quart J Roy Meteorol Soc 116:637–670

Steyn DG (2003) Scaling the vertical structure of sea breezes revisited. Boundary-Layer Meteorol 107:177–188

Thunis P, Clappier A (2000) Formulation and evaluation of a non-hydrostatic meso-scale vorticity model (TVM). Mon Wea Rev 128:3236–3250

Vergeiner I, Dreiseitl E (1987) Valley winds and slope winds-observations and elementary throughts. Meteorol Atmos Phys 36:264–286

Vergeiner I (1991) Comments on Large-eddy simulation of the up-slope boundary-layer by Ulrich Schumann. Quart J Roy Meteorol Soc 117:1371–1372

Ye ZJ, Segal M, Pielke RA (1987) Effects of atmospheric thermal stability and slope steepness on the devlopment of daytime thermally induced upslope flow. J Atmos Sci 44:3341–3354